Available online at www.sciencedirect.com
ScienceDirect
Measurement 39 (2006) 947–958
Measurement
www.elsevier.com/locate/measurement

Computer simulation of a piezoelectric angular rate sensor

Saulius Kausinis [a,*], Rimantas Barauskas [b]

[a] Department of Engineering Mechanics, Kaunas University of Technology, K. Donelaicio Str. 73, LT-44029, Lithuania
[b] Department of System Analysis, Kaunas University of Technology, Studentu Str. 50-407, LT-51368, Kaunas, Lithuania

Available online 15 April 2006

Abstract

The paper presents the finite element (FE) modeling of operation of a rotational motion sensor that uses a balanced oscillator (tuning fork) to sense the angular rate. The 3D FE model has been employed for the investigation of the dynamic properties of the sensor. The sensitivity functions have been obtained for adjusting the geometric parameters of the quartz element in order to achieve the desired values of natural frequencies. The performance of dynamic computations has been improved by truncating the dynamic contributions of higher modes of the vibrating structure.

Results are presented in terms of performance characteristics of the sensor against the design parameters in various modes of operation.

Keywords: Finite elements; Piezoelectric sensor; Angular rate

1. Introduction

MEMS[1]-based measurement units on a single chip offer major advantages in terms of size, weight and cost over conventional systems. It is envisioned that MEMS is an enabling technology that may potentially offer improved systems' performance as well as extended functionalities and enhanced lifetime.

Some specific vehicle applications of the MEMS motion detection devices encounter unique challenges due to both the demanding operational and environmental standards and requirements for stringent reliability and performance degradation.

MEMS technology has the potential to mitigate challenges posed by future developments of Inertial Measurement Units. They include miniaturisation, reduced cost of fabrication and real-time control.

Methods of development and analysis of such systems require special knowledge and approaches to mathematical modelling of the behaviour of systems and to the evaluation of their properties. The finite element method applied to piezoelectric transducers provides highly adequate dynamic models. The models describe the fundamental principles underlying the measurement systems, as well as, provide the means of treatment of deviations and uncertainties based on the analysis of instrument's structure and the effects of sensitivity to parameters variations and external influences.

Systematic approaches to mathematical modelling of sensors are extensively discussed in [1].

* Corresponding author. Tel.: +370 37 323855; fax: +370 37 324144.
E-mail address: Saulius.Kausinis@ktu.lt (S. Kausinis).
[1] MEMS – micro-electro-mechanical systems.

0263-2241/$ - see front matter © 2006 Elsevier Ltd. All rights reserved.
doi:10.1016/j.measurement.2006.04.001

The application of the FE method for modal analysis of piezoelectric resonators is described in [2]. The variational formulation of the problem is based on the physical description of the behaviour of piezoelectric structures. The governing equations of the piezoelectric continua are based on Newton's laws of motion and the quasi-static approximation of Maxwell's equation.

The piezoelectric angular rate sensors employ the phenomenon of the Coriolis acceleration. In the sensor under consideration an oscillatory motion of the vibrating structure is coupled from the primary vibrating mode into the secondary mode as the sensor experiences the angular motion.

In [3] the FE analysis has been used for modelling the angular rate sensor built on the base of the shell resonator technology. In particular, the sensitivity of the sensor to external vibration inputs has been studied.

A micro-machined angular rate sensor with two rotary vibration modes has been described in [4]. The mechanical sensor element consists of comb-shaped drives, which build the spokes of the inner wheel, and of the outer rectangular structure which is called the secondary oscillator. Finite element simulation has been applied to both the analysis of the shock resistance of the mechanical system and for modelling of the rotary vibration modes of the structure.

The use of a simple mechanical coupling model and FE analysis in order to optimise the design of the sensor and to reduce the offset output of the H-shape resonator is presented in [5]. The results of the analysis demonstrated a strong correlation between the geometric shape of the vibrator and the ratio between the differing excitation and detection frequencies.

In this work we provide the analysis and design tools for MEMS devices performance evaluation by using the micro-gyro as an example. We introduce a 3D finite element computational model and software tools allowing to investigate the dynamic properties of the balanced oscillator as a constituent part of the angular rate sensor and to appreciate its parametric sensitivity. A linear piezoelectric vibration finite element model has been extended in order to take into account the rigid body rotation of the transducer and to present the coupling effect between in-plane and out-of plane modes caused by Coriolis forces. The comparative modelling results are being reported.

2. Basic principles

There are many practical implementations of the angular rate sensors the principle of operation of which is based on the high-frequency structural vibrations. They can be embodied as simple oscillators, balanced oscillators or shell resonators [3]. In the GyroChip sensor family balanced oscillators are employed in order to detect and measure the angular rate. The physical principles of the operation and performance specifications of the sensor are presented in [6,7] as well as on the web site http://www.systron.com.

The sensor has found wide applications in the automotive, aerospace, defence, industrial, commercial, and medical industries. It consists of a micro-miniature quartz transducer shaped as a double-ended tuning fork and of the supporting structure. Both are fabricated chemically from a single wafer of the mono-crystalline piezoelectric quartz, Fig. 1. Due to a single-crystal implementation, the quartz is stable under temperature changes during very long operation time and mechanical impacts.

As the reference frame rotates about the sensor's longitudinal axis Oz, the tines vibrating in xOz plane experience simultaneously the Coriolis acceleration directed along axis Oy that is directly proportional to the angular rate of rotation of the reference frame.

The drive tines constitute the active part of the sensor. They are driven to vibrate at precisely prescribed amplitude. Each tine will experience the Coriolis force acting on it as:

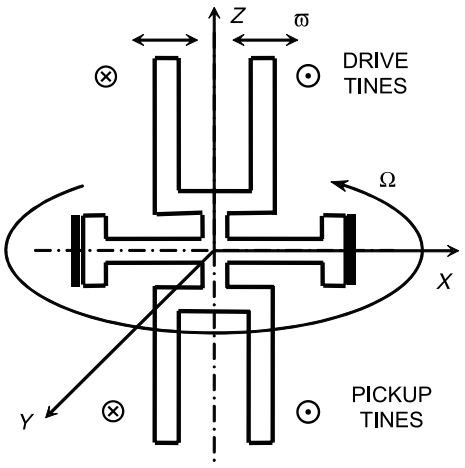

Fig. 1. Balanced tuning fork-shaped quartz resonator of the sensor.

$$F = 2 \cdot m \cdot \Omega \cdot V_{\mathrm{r}}, \tag{1}$$

where m – mass of the tine, V_{r} – instantaneous radial velocity, Ω – the input angular rate.

The Coriolis force is perpendicular to both the input rate and the instantaneous radial velocity. As the two drive tines move in the opposite directions, the resultant forces acting on them are perpendicular to the plane of the fork and of opposite directions. As a result, a torque proportional to the input rotational rate is produced.

The pickup tines serve as a sensing part of the sensor. They are responding to the oscillating torque by performing the out-of-plane vibration and produce the output signal proportional to the angular rate.

3. Lumped-parameters model

The simplest lumped-parameters model of the angular rate sensor is presented in Fig. 2 [8,9]. It contains a mass able to vibrate along Ox and Oy directions independently. The system is mounted inside of a rotating frame, the angular rate of which is being measured. The coupling between the vibrations in the two directions takes place because of the Coriolis acceleration that is directed along Oy as a consequence of the rotation of the frame about Oz and the linear motion of the mass along Ox.

The dynamic equation of the system in Fig. 2 can be presented as

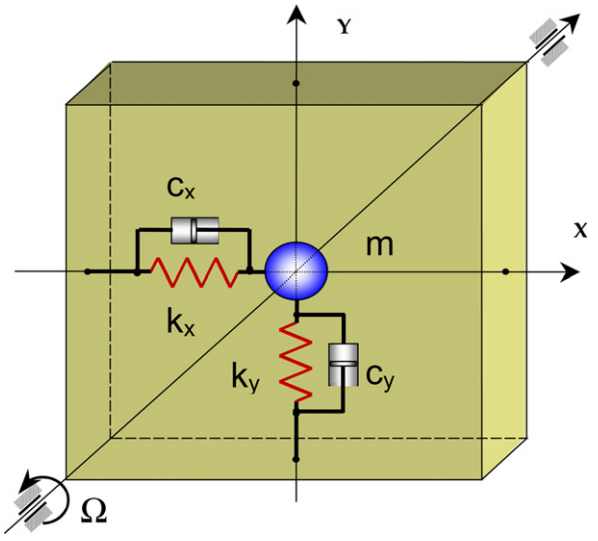

Fig. 2. Lumped-mass model of the angular velocity sensor.

$$\begin{Bmatrix} \ddot{x} \\ \ddot{y} \end{Bmatrix} + 2\begin{bmatrix} \vartheta\omega_x & -\Omega \\ \Omega & \vartheta\omega_y \end{bmatrix}\begin{Bmatrix} \dot{x} \\ \dot{y} \end{Bmatrix} + 2\begin{bmatrix} \omega_x^2 & 0 \\ 0 & \omega_y^2 \end{bmatrix}\begin{Bmatrix} x \\ y \end{Bmatrix} = \begin{Bmatrix} \hat{f}\cos\omega t \\ 0 \end{Bmatrix}, \tag{2}$$

where $x(t), y(t), \dot{x}, \dot{y}, \ddot{x}, \ddot{y}$ – displacements, velocities and accelerations of the mass in Ox and Oy directions, ϑ_x, ϑ_y – damping ratios of vibrations, ω_x, ω_y – natural frequencies of vibrations along Ox and Oy, $\hat{f}$ – excitation force amplitude along Ox, ω – excitation frequency, Ω – angular velocity of the frame. The skew-symmetric terms Ω and $-\Omega$ appear in the gyroscopic part of the matrix and take into account the Coriolis forces. Here we neglect the spin-softening effects caused by the centripetal inertia force as oscillation amplitudes of the vibrating mass are very small.

The solution of system (2) is obtained in terms of amplitudes of harmonic vibrations. The main dynamic properties of the system are presented by the relationships in Figs. 3 and 4.

Fig. 3 presents the vibration amplitude against the excitation frequency relationships (AFCH) for different values of the ratio of natural frequencies ω_y/ω_x. By choosing the appropriate value of ω_y/ω_x, a plateau on the AFCH of Oy vibrations can be obtained. In this way, nearly constant values of the vibration amplitudes are ensured in a rather wide excitation frequency range in the vicinity of the resonance.

Fig. 4 presents the relationship of the response amplitudes along Oy and phases of vibration against the angular rate of the rotation of the reference frame for the example system having the damping ratio 0.02 and the natural frequency ratio $\omega_y/\omega_x = 1.03$.

In the range of angular rates $-0.01\omega_x < \Omega < 0.01\omega_x$ nearly linear relationships can be observed. The reverse of the direction of the angular rate leads to the immediate reverse of the sign of the phase of Oy vibrations.

4. Finite element model

The tuning fork is a vibrating piezoelectric plate of the complex geometric shape the side surfaces of which are laminated by electrodes enabling to create an electric field inside of the material. The differential equations governing the behaviour of the piezoelectric continuum are the Newton's laws of motion and the quasi-static approximation of the Maxwell's equation.

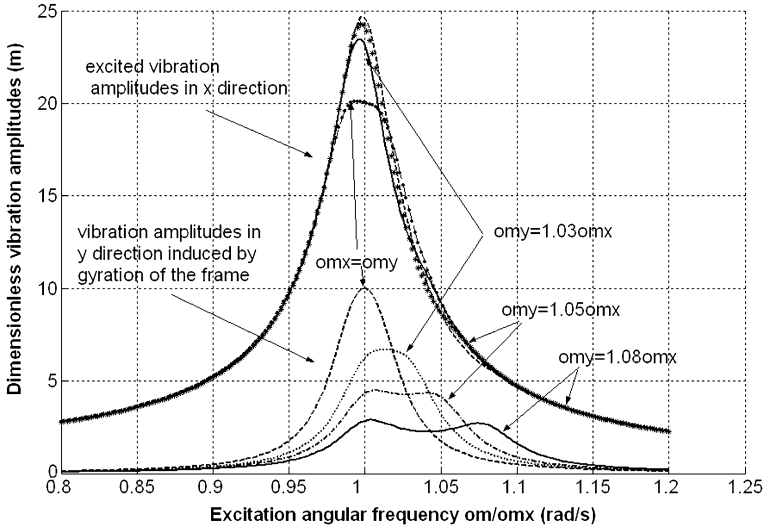

Fig. 3. Amplitude frequency characteristics of the lumped mass model at different values of the natural frequency ratio ω_y/ω_x.

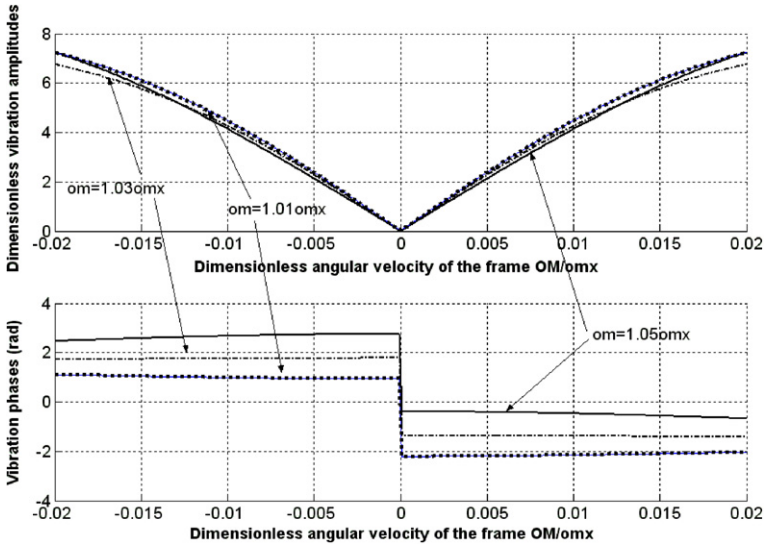

Fig. 4. Response amplitudes and phases of the lumped mass model against the angular velocity of the rotation of the frame at $\omega_y/\omega_x = 1.03$; $\vartheta_x = \vartheta_y = 0.02$.

Elastic vibrations of a body are described by means of the differential equations in its volume V and boundary conditions on its surface S as

$$\begin{aligned} &[\mathbf{A}]^{\mathrm{T}}\{\boldsymbol{\sigma}\} + \{\mathbf{b}\} = \rho\{\ddot{\mathbf{u}}\}, \quad \in V \\ &\{\mathbf{t}\} = [\mathbf{A}_s]^{\mathrm{T}}\{\boldsymbol{\sigma}\}, \quad \in S \end{aligned} \tag{3}$$

where $\{\boldsymbol{\sigma}\}$ – stress tensor in Voigt's notation, $\{\mathbf{b}\}$ – body force vector, $\{\mathbf{t}\}$ – tractions vector on surface S, $\{\mathbf{u}\}$ – displacement vector of any point of the body, ρ – density of the material, $[\mathbf{A}]$ – differential operator, $[\mathbf{A}_s]$ – matrix containing components of unit normal vector $\{\mathbf{n}\}$ to surface S. In the 2D case we have

$$[\mathbf{A}] = \begin{bmatrix} \frac{\partial}{\partial x} & 0 \\ 0 & \frac{\partial}{\partial y} \\ \frac{\partial}{\partial y} & \frac{\partial}{\partial x} \end{bmatrix}, \quad [\mathbf{A}_s] = \begin{bmatrix} n_x & 0 \\ 0 & n_y \\ n_y & n_x \end{bmatrix}.$$

The constitutive equation of piezoelectricity relating stresses, strains, electric field and electric displacement components reads as

$$\begin{cases} \{\boldsymbol{\sigma}\} = [\mathbf{c}^{\mathrm{E}}]\{\boldsymbol{\varepsilon}\} - [\mathbf{e}]\{\mathbf{E}\}, \\ \{\mathbf{D}\} = [\mathbf{e}]^{\mathrm{T}}\{\boldsymbol{\varepsilon}\} - [\boldsymbol{\kappa}]\{\mathbf{E}\}, \end{cases} \tag{4}$$

where $\{\mathbf{E}\}$ – electric field vector, $\{\mathbf{D}\}$ – dielectric displacement vector, $[\mathbf{c}^{\mathrm{E}}]$ – stiffness tensor at constant electric field value, $[\mathbf{e}]$ – piezoelectric tensor, $[\boldsymbol{\kappa}]$ – dielectric tensor. In many practical situations the electric field created in the material may be considered as known. In this case the piezoelectric phenomena in the plate are governed by the single linear piezoelectricity equation as

$$\{\boldsymbol{\sigma}\} = [\mathbf{c}^{\mathrm{E}}]\{\boldsymbol{\varepsilon}\} - [\mathbf{e}]\{\mathbf{E}\}. \tag{5}$$

As relative displacements of the tuning fork with respect to the rotating reference frame are being considered, the full acceleration $\{\mathbf{a}_{\mathrm{F}}\} = \{\mathbf{a}\} + \{\mathbf{a}_{\mathrm{N}}\} + \{\mathbf{a}_{\mathrm{T}}\} + \{\mathbf{a}_{\mathrm{C}}\}$ should be used in the virtual work equation of the finite element as

$$\int_V \delta\{\boldsymbol{\varepsilon}\}^{\mathrm{T}}\{\boldsymbol{\sigma}\}\mathrm{d}V + \int_V \rho\delta\{\mathbf{u}\}^{\mathrm{T}}\{\mathbf{a}_{\mathrm{F}}\}\mathrm{d}V = \delta\{\mathbf{U}\}^{\mathrm{T}}\{\mathbf{R}\}, \tag{6}$$

where symbol δ denotes the virtual quantity, $\{\mathbf{u}\} = [\mathbf{N}]\{\mathbf{U}\}$ – the displacement vector of a particle inside the finite element expressed in terms of the form function matrix $[\mathbf{N}]$ and the nodal displacement vector $\{\mathbf{U}\}$, ρ – density of the material, $\{\mathbf{R}\}$ – vector of nodal interaction forces, $\{\mathbf{a}\}$ – relative acceleration with respect to the rotating frame; $\{\mathbf{a}_{\mathrm{N}}\}$, $\{\mathbf{a}_{\mathrm{T}}\}$ – normal and tangential accelerations due to the rotation of the frame; $\{\mathbf{a}_{\mathrm{C}}\}$ – Coriolis acceleration.

The structural dynamic equation of the finite element of the H shape vibrator is obtained as [8,9]:

$$\begin{aligned} &[\mathbf{M}]\{\ddot{\mathbf{U}}\} + 2\Omega[\mathbf{G}]\{\dot{\mathbf{U}}\} + ([\mathbf{K}] - \Omega^2[\mathbf{K}_1] + \varepsilon[\mathbf{G}])\{\mathbf{U}\} \\ &\quad = \{\mathbf{R}\} + \{\mathbf{F}\} + \Omega^2[\mathbf{K}_1]\{\mathbf{X}\} - \varepsilon[\mathbf{G}]\{\mathbf{X}\}, \end{aligned} \tag{7}$$

where $[\mathbf{G}] = \int_V \rho[\mathbf{N}]^{\mathrm{T}}\begin{bmatrix} 0 & -1 & 0 \\ 1 & 0 & 0 \\ 0 & 0 & 0 \end{bmatrix}[\mathbf{N}]\mathrm{d}V$ – gyroscopic matrix, $[\mathbf{K}_1] = \int_V \rho[\mathbf{N}]^{\mathrm{T}}\begin{bmatrix} 1 & 0 & 0 \\ 0 & 1 & 0 \\ 0 & 0 & 0 \end{bmatrix}[\mathbf{N}]\mathrm{d}V$ – centripetal force matrix, $[\mathbf{M}] = \int_V \rho[\mathbf{N}]^{\mathrm{T}}[\mathbf{N}]\mathrm{d}V$, $[\mathbf{K}] = \int_V [\mathbf{B}]^{\mathrm{T}}[\mathbf{c}^{\mathrm{E}}][\mathbf{B}]\mathrm{d}V$ – correspondingly mass and stiffness matrices, $\{\mathbf{F}\} = \int_V [\mathbf{B}]^{\mathrm{T}}[\mathbf{e}]\{\mathbf{E}\}\mathrm{d}V$ – nodal excitation forces due to the inverse piezoelectric effect, $\{\mathbf{X}\}$ – vector of nodal coordinates of the finite element, Ω and ε correspondingly are the angular rate and angular acceleration of the reference frame rotation about Oz axis.

The energy dissipation in piezoelectric transducers may be caused by mechanical, piezoelectric and electrical phenomena taking place during the vibration. The true mechanism of the energy dissipation is very complex. However, as the first approximation it may be reasonably assumed that the damping phenomena are caused mainly by the hysteresis loop in the relation $\boldsymbol{\sigma}(\boldsymbol{\varepsilon})$ presented by Eq. (5). In harmonic vibration analysis the hysteresis phenomena are generally described by introducing complex values of stiffness coefficients as $[\mathbf{c}^{\mathrm{E}}] = [\bar{\mathbf{c}}^{\mathrm{E}}](1 + j\eta_{\mathrm{M}})$ where η_{M} is referred to as the mechanical dissipation factor. The physical meaning of η_{M} is the tangent of the phase shift angle between the stress and the strain caused by the hysteresis phenomena during the harmonic vibration of the piezoelectric transducer.

By employing the complex value of $[\mathbf{c}^{\mathrm{E}}]$ we assume that the dynamic analysis is carried out in the frequency domain and consequently the stiffness matrix of the transducer is presented in the complex form as $[\mathbf{K}](1 + j\eta_{\mathrm{M}})$. Mathematically the same effect is obtained by introducing the damping term $[\mathbf{C}]\{\dot{\mathbf{U}}\}$ into Eq. (7), where $[\mathbf{C}] = \eta_{\mathrm{M}}[\mathbf{K}]$ is referred to as the proportional damping matrix. A general form of the proportional damping matrix is presented as $[\mathbf{C}^e] = \alpha[\mathbf{M}^e] + \beta[\mathbf{K}^e]$, where coefficients α, β may be easily determined if two values of the dynamic amplification factor of the vibrations corresponding to two different vibration frequencies are known. Such simplified dissipation models can be used in practical computations only if damping forces are small. Small damping is an inherent feature of resonant piezoelectric vibrating systems considered in this study. Their dynamic amplification factor may reach values 50–1000.

The finite element model has been implemented and modal analysis has been performed in ANSYS finite element software by using shell elements SHELL43 and material parameters corresponding to stiffness tensor $[\mathbf{c}^{\mathrm{E}}]$. The finite element mesh can be seen in Fig. 5. The modal errors caused by the discretization have been estimated by comparing the modal results obtained by considering models of different mesh refinements. It has been demonstrated that the mesh presented in Fig. 5 provides satisfactory results in the range of modal frequencies necessary for analyses performed in this study.

By the use of finite element analysis both the operation specifics of the sensor and the quantitative evaluation of the relationship of the output signal against the angular rate of the outer frame have been carried out.

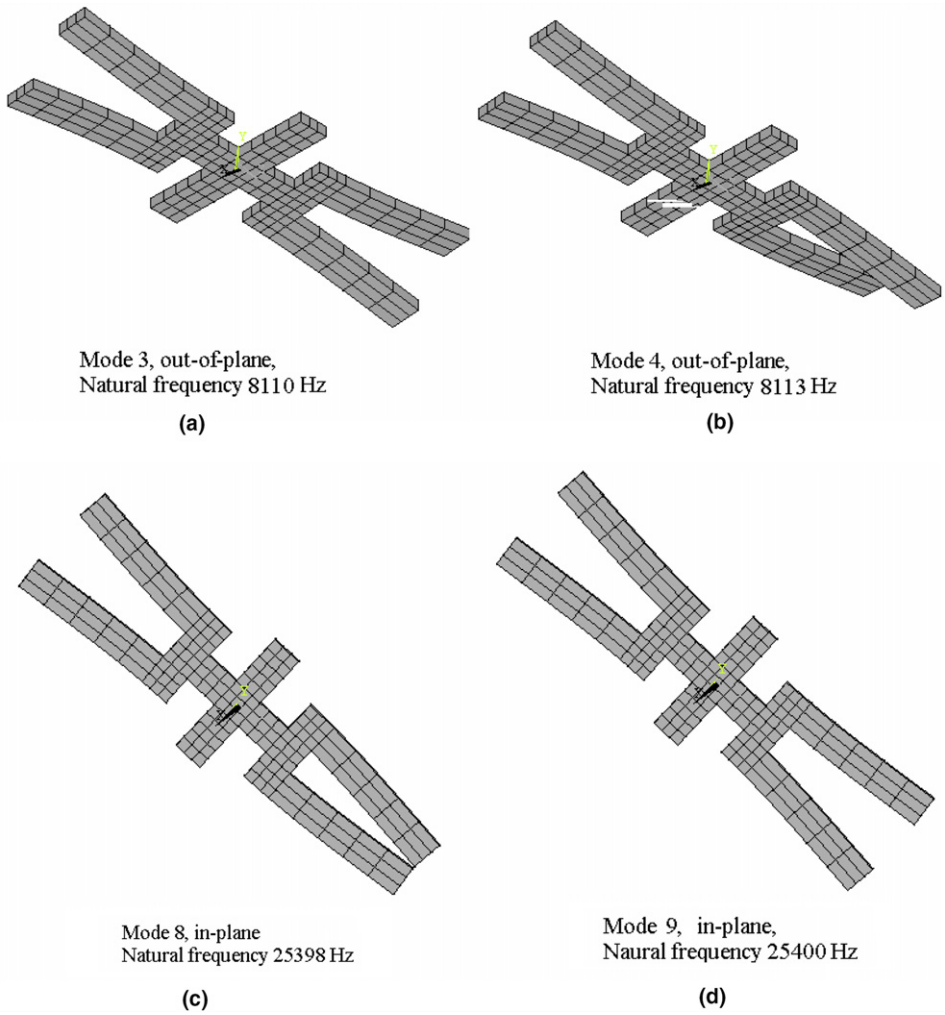

Fig. 5. (a,b) The 3 and 4 mode shapes of the vibrating structure. (c,d) The 8 and 9 mode shapes of the vibrating structure.

By using the finite element model of the tuning fork-shaped quartz transducer we calculate a finite number of modes of a non-rotating transducer. They are obtained by solving the characteristic equation as

$$([\mathbf{K}] - \omega^2[\mathbf{M}])\{\mathbf{U}\} = 0. \quad (8)$$

A typical set of geometrical values of the transducer gives the modal frequencies the lower range of which are presented in Table 1.

The fundamental vibration modes of interest are the 3rd, 4th, 8th and the 9th. They play the key role in the resonant dynamic behavior of the angular rate sensor and provide the in-plane and out-of-plane vibration coupling of the transducer rotating about the *Oz* axis. The shapes of the modes are presented in Fig. 5.

The 3rd and 4th modes situated closely in the frequency range exist only if the ends of the horizontal bar (see Fig. 1) are constrained rigidly.

5. Parametric sensitivity

The tuning fork-shaped transducer is a mechanical vibrating system with high value of the dynamic amplification factor. Its performance and dynamic features depend substantially upon modal frequencies and shapes of vibration. The influence of the design parameters upon the modal properties of the transducer has been investigated by employing the sensitivity functions.

A sensitivity function denotes the sensitivity of the output values of the system to the variations of the system's design parameters. As the design

Table 1
Lower range of modal frequencies of the fork

Mode number	Natural frequency (Hz)	Basic feature of the natural form
1	3529	Out-of-plane, torsion of the supporting bar about Ox
2	4048	Out-of-plane, I bending mode symmetrical to Ox
3	8110	Out-of-plane, bending of fork legs, symmetrical to Ox and anti-symmetrical to Oz
4	8113	Out-of-plane, bending of fork legs, anti-symmetrical to Ox and Oz
5	11,215	In-plane, torsion of the center of the cross about Oy
6	12,052	In-plane, bending of the neck symmetrical to Ox
7	25,085	Out-of-plane, II bending mode along Oz
8	25,398	In-plane, bending of the legs symmetrical to Oz and anti-symmetrical Ox
9	25,400	In-plane, bending of the legs anti-symmetrical to Oz and symmetrical to Ox
10	27,183	Out-of-plane, III bending mode along Oz

parameters in this study we analyze the geometric values presented in Fig. 6. The finite element matrices of the transducer can be presented as functions $[\mathbf{K}(b_i)]$, $[\mathbf{M}(b_i)]$ of design parameters b_i of the vibrating structure [9]. The relations between small variations of the design parameters and corresponding variations of modal frequencies are obtained by using the characteristic Eq. (8). The first variation of (8) gives the following relations, [9]:

$$\partial\{\zeta_i\} = [\mathbf{C}_i]\partial\{\mathbf{b}\}, \tag{9}$$

where $[\mathbf{C}_i] = \{\mathbf{y}_i\}^{\mathrm{T}}\left(\frac{\partial[\mathbf{K}]}{\partial\{\mathbf{b}\}} - \zeta_i\frac{\partial[\mathbf{M}]}{\partial\{\mathbf{b}\}}\right)\{\mathbf{y}_i\}$ is the matrix of sensitivity coefficients, $\zeta_i = \omega_i^2$ – square of the ith modal frequency, $\{\mathbf{y}_i\}$ – the vector describing the ith modal shape.

The first variation of (8) gives the following relations:

$$\left(\frac{\partial[\mathbf{K}]}{\partial\{\mathbf{b}\}} - \zeta_i\frac{\partial[\mathbf{M}]}{\partial\{\mathbf{b}\}}\right)\{\mathbf{y}_i\}\partial\{\mathbf{b}\} + ([\mathbf{K}] - \zeta_i[\mathbf{M}])\partial\{\mathbf{y}_i\} - \partial\zeta_i[M]\{\mathbf{y}_i\} = 0;$$

$$2\{\mathbf{y}_i\}^{\mathrm{T}}[\mathbf{K}]\{\mathbf{y}_i\} + \{\mathbf{y}_i\}^{\mathrm{T}}\frac{\partial[\mathbf{K}]}{\partial\{\mathbf{b}\}}\{\mathbf{y}_i\}\partial\{\mathbf{b}\} - \partial\zeta_i = 0;$$

$$2\{\mathbf{y}_i\}^{\mathrm{T}}[\mathbf{M}]\{\mathbf{y}_i\} + \{\mathbf{y}_i\}^{\mathrm{T}}\frac{\partial[\mathbf{M}]}{\partial\{\mathbf{b}\}}\{\mathbf{y}_i\}\partial\{\mathbf{b}\} = 0. \tag{10}$$

By taking into account the inherent properties of modal shapes of a structure as

$$\{\mathbf{y}_i\}^{\mathrm{T}}[\mathbf{K}]\{\mathbf{y}_i\} = [\mathbf{diag}(\zeta_i)]; \quad \{\mathbf{y}_i\}^{\mathrm{T}}[\mathbf{M}]\{\mathbf{y}_i\} = [\mathbf{I}], \tag{11}$$

where $[\mathbf{I}]$ – the identity matrix, the sensitivity functions of natural frequencies and shapes to parameter variations can be expressed as

$$\partial\{\mathbf{y}_i\} = [\mathbf{A}_i]^{-1}[\mathbf{B}_i]\partial\{\mathbf{b}\}; \quad \partial\{\zeta_i\} = [\mathbf{C}_i]\partial\{\mathbf{b}\}, \tag{12}$$

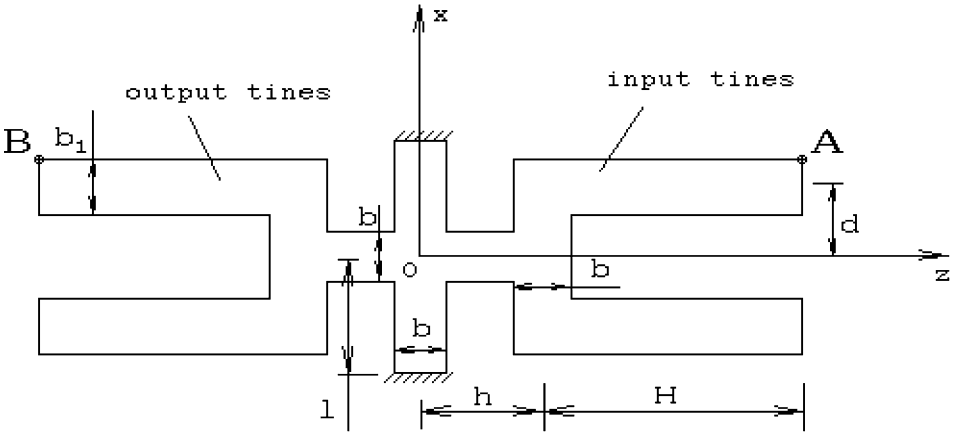

Fig. 6. Geometric parameters of the transducer.

where

$$[\mathbf{A}_i] = [\mathbf{K}] - \zeta_i[\mathbf{M}] - 2[\mathbf{M}]\{\mathbf{y}_i\}\{\mathbf{y}_i\}^{\mathrm{T}}[\mathbf{K}];$$

$$[\mathbf{B}_i] = \frac{\partial[\mathbf{K}]}{\partial\{\mathbf{b}\}} - \zeta_i\frac{\partial[\mathbf{M}]}{\partial\{\mathbf{b}\}} - 2[\mathbf{M}]\{\mathbf{y}_i\}\{\mathbf{y}_i\}^{\mathrm{T}}\frac{\partial[x]}{\partial\{\mathbf{b}\}};$$

$$[\mathbf{C}_i] = \{\mathbf{y}_i\}^{\mathrm{T}}\left(\frac{\partial[\mathbf{K}]}{\partial\{\mathbf{b}\}} - \zeta_i\frac{\partial[\mathbf{M}]}{\partial\{\mathbf{b}\}}\right)\{\mathbf{y}_i\}.$$

The sensitivity functions obtained can be further employed to the shape optimisation of the tuning fork in order to satisfy the necessary ratio between the working resonant frequencies and to ensure the necessary modal shapes. They enable to find the most effective structural shape modifications ensuring the desired change of modal properties.

The analysis of the sensitivity coefficients obtained indicates that the stiffness of the supporting *Ox* bar (see Fig. 6) described by its length *l* and width *b* has the main influence upon the values of the 3rd and 4th modal frequencies. The plot of the values of the two frequencies against the value of parameter *l* (half length of the supporting bar) is presented in Fig. 7.

At $l \approx 1.54$ mm natural frequencies of the 3rd and 4th modes are equal. This circumstance requires a special attention during the dynamic analysis as here the magnitudes of the two modal frequencies may interchange as a result of a small variation of *l*.

6. Reduction of the dynamic equations

The modes presented in Section 2 describe the dynamic properties of the transducer in the non-rotating reference frame. If the rotation of the frame takes place, the modes of vibration change depending upon the angular rate of rotation. They are expressed in complex numbers, and the physical interpretation of them becomes quite complicated. As Eq. (7) is linear, steady harmonic vibration laws of the transducer at a prescribed harmonic excitation and angular rate of the rotation of the reference frame can be easily found in terms of amplitudes of vibration. However, in case of moderate angular velocities of rotation of the frame the modal coupling and resonance phenomena of the transducer in the rotating reference frame can be much better understood by expressing the equations in modal coordinates of the non-damped and non-rotating structure, the vibration modes of which have a simple engineering interpretation. Moreover, the aim of having the modal properties of a non-rotating structure as target functions in geometrical design of the transducer can be regarded as more natural and convenient.

Let $\omega_1, \omega_2, \ldots, \omega_n$ be the modal frequencies and matrix [**Y**] contain in its columns the modal shapes of vibration of the non-rotating transducer. By neglecting the effects caused by angular acceleration and centripetal forces, the steady vibration of the

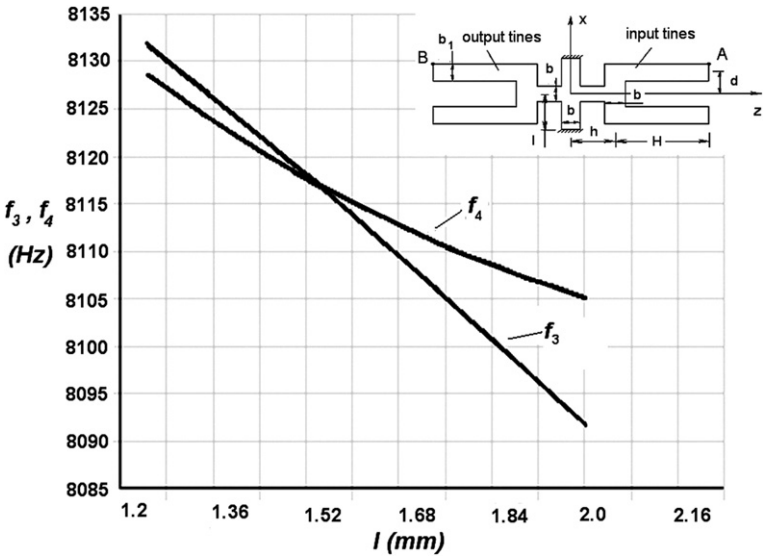

Fig. 7. Modal frequencies of the 3rd and 4th modes vs. length *l* of the *Ox* supporting bar of the transducer.

transducer in the rotating reference frame is governed by the equation expressed in terms of modal displacements $\{\mathbf{z}\}$ as

$$\{\ddot{\mathbf{z}}\} + [\mathbf{diag}(\mu)]\{\dot{\mathbf{z}}\} + [\mathbf{diag}(\omega^2)]\{\mathbf{z}\} = -2\Omega[\mathbf{Y}]^{\mathrm{T}}[\mathbf{G}][\mathbf{Y}]\{z\} + [\mathbf{Y}]^{\mathrm{T}}\{\mathbf{F}\}, \quad (13)$$

where modal displacements $\{\mathbf{z}\}$ are related to nodal displacements of the structure as $\{\mathbf{U}\} = [\mathbf{Y}]\{\mathbf{z}\}$, the modal damping coefficients $\mu_1, \mu_2, \ldots, \mu_n$ are obtained as $\mu_i = \alpha + \beta\omega_i^2$, and the properties of modal shapes as $[\mathbf{Y}]^{\mathrm{T}}[\mathbf{M}][\mathbf{Y}] = [\mathbf{I}]$, $[\mathbf{Y}]^{\mathrm{T}}[\mathbf{K}][\mathbf{Y}] = [\mathbf{diag}(\omega^2)]$ have been employed. It should be noticed that modal Eqs. (13) are coupled, as matrix $[\mathbf{Y}]^{\mathrm{T}}[\mathbf{G}][\mathbf{Y}]$ is non-diagonal.

Eq. (13) can be simplified by neglecting the dynamic contributions of higher modes of the transducer, [10]. We partition the modes and modal displacements into two sets so that the displacement vector can be presented as $\{\mathbf{U}\} = [\mathbf{Y}_1]\{\mathbf{z}_1\} + [\mathbf{Y}_2]\{\mathbf{z}_2\}$, and truncate the terms corresponding to inertial and damping forces of the second modal set. Finally the following equation in terms of modal displacements of only first set is obtained:

$$\{\ddot{\mathbf{z}}_1\} + ([\mathbf{diag}(\mu_1)] + 2\Omega[\mathbf{Y_1}]^{\mathrm{T}}[\mathbf{G}][\mathbf{Y}_1])\{\dot{\mathbf{z}}_1\} + [\mathbf{diag}(\omega_1^2)]\{\mathbf{z}_1\} = -2\Omega[\mathbf{Y}_1]^{\mathrm{T}}[\mathbf{G}][\mathbf{S}_k]\{\dot{\mathbf{F}}\} + [\mathbf{Y}_1]^{\mathrm{T}}\{\mathbf{F}\}, \quad (14)$$

where $[\mathbf{S}_k] = [\mathbf{K}]^{-1} - [\mathbf{Y}_1][\mathbf{diag}(1/\omega_1^2)][\mathbf{Y}_1]^{\mathrm{T}}$ is the quasistatic compliance matrix of higher modes.

Modal frequencies and shapes of the non-rotating transducer are obtained by using the finite element software system ANSYS as described in Section 4 and exported to the FORTRAN program developed by us in order to calculate the dynamic response of the transducer situated in the reference frame rotating at angular rate Ω. Calculations were performed in modal coordinates of the non-rotating transducer by taking into account the coupling terms between the modes caused by the gyroscopic matrix [**G**]. All computations have been performed on Pentium IV 1.7 MHz personal computer.

The accuracy of the solution depends upon the number of modes taken into consideration. We may always obtain the exact solution when solving equations with all modes participating with their dynamic contributions. However, if the solution close to the exact can be obtained when taking into account the dynamic contributions of only few modes, such modes are of primary importance for ensuring the operation law of the angular rate sensor.

Fig. 8 presents the amplitude frequency characteristics (AFCH) of the characteristic points (A) and (B) (Fig. 6) on the input (driving) and output (pickup) tines of the tuning fork by taking first 4 modes, first 9 modes and the full dynamic model.

The amplitudes are presented in the dimensionless form

$$\overline{U} = \frac{Uc_{11}^{\mathrm{E}}}{e_{31}Ed},$$

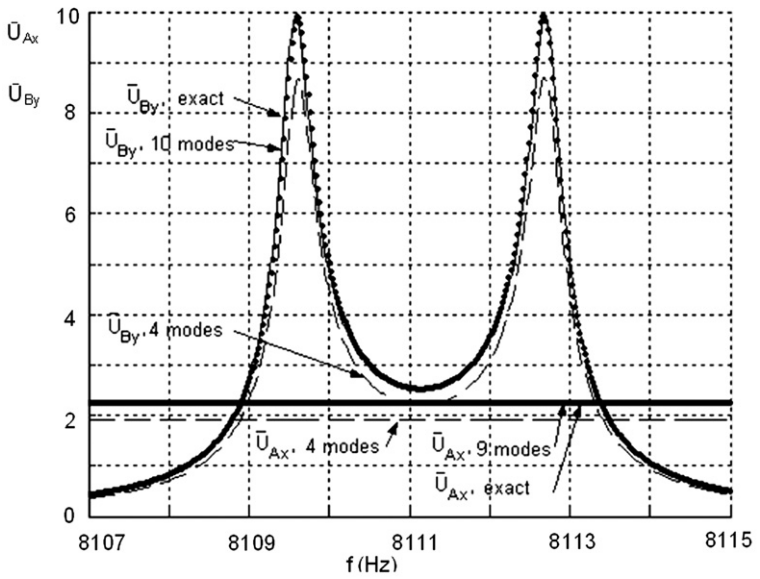

Fig. 8. Amplitude–frequency characteristic of the response of the vibrating structure; $\overline{U}_{\mathrm{Ax}}, \overline{U}_{\mathrm{By}}$ – the dimensionless vibration amplitudes of points A and B of the transducer in Ox and Oy directions.

where c_{11}^{E} – Young's modulus, e_{31} – piezoelectric coefficient, E – electric field strength, d – geometric parameter of the transducer shown in Fig. 6. As reference displacement here we consider the static elongation $\frac{e_{31}Ed}{c_{11}^{E}}$ of the bar connecting the tines of the fork affected by the electric voltage equal to the amplitude of the harmonic excitation of the fork. Two peaks on the AFCH of amplitude $\overline{U}_{By}$ correspond to two neighbouring 8th and 9th modes. AFCH of $\overline{U}_{Ax}$ contains no peaks as the modal frequencies of in-plane modes (the dominant vibrations of them are directed along Ox) are situated far from the frequency range presented in Fig. 8.

The detailed analysis of the influence of modes by adding them one by one to the dynamic model leads to the conclusion that the 9×9 reduced dynamic model obtained by taking into account the dynamic contributions of only first 9 modes is accurate enough and can be used instead of the full 1326×1326 original model. It should be noticed that 8th and 9th dynamic modal contributions though excited far below the resonance are important for proper representation of the dynamic features of the system.

The comparison of the results obtained by using the reduced and full models demonstrates their good agreement. The reduced model runs 50–100 times faster and saves the computation time considerably when obtaining the amplitude- and phase-frequency characteristics that require multiple calculations of the forced harmonic response.

7. Analysis of the dynamic behaviour

In order to perform its function as the sensitive element of the angular rate meter, the tuning fork-shaped quartz transducer is excited by means of the applied electric voltage over one half of the fork (input tines). The frequency of excitation of the fork is close to the natural frequencies of resonant out-of-plane modes three and four, though the modes are not excited because of the in-plane action of the electromechanical excitation forces.

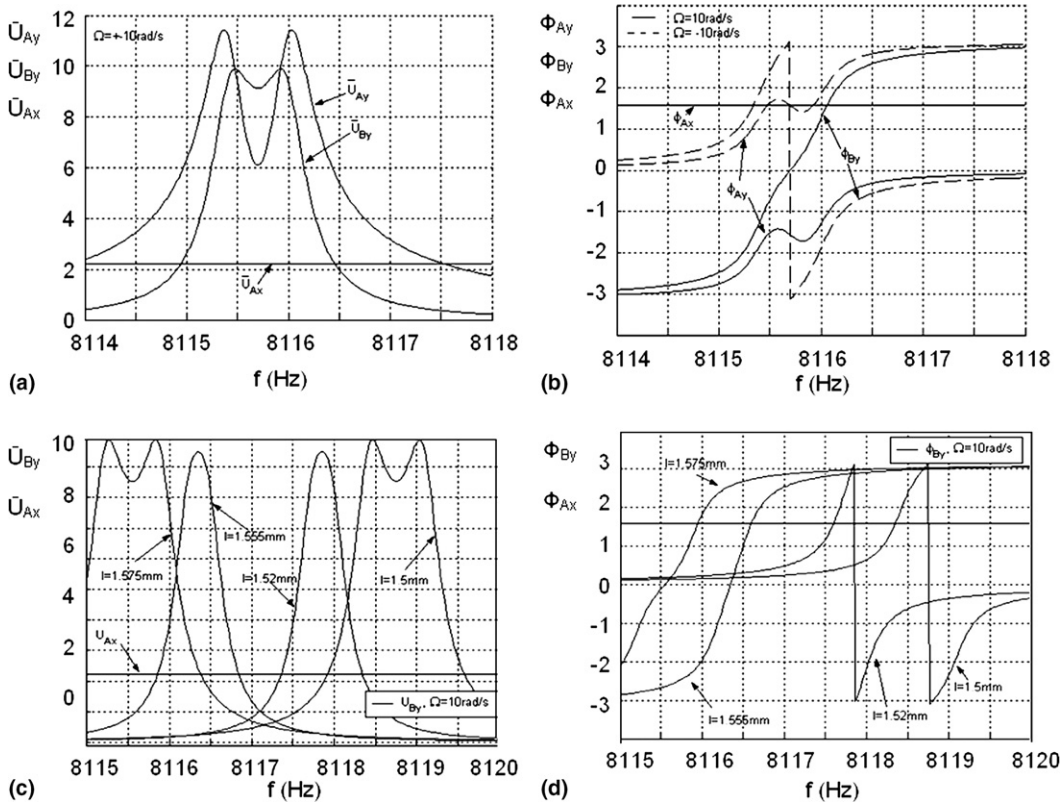

Fig. 9. Effects of separation of modal frequencies f_3 and f_4 on the frequency response of the transducer. (a,c) Amplitude–frequency characteristics; (b,d) amplitude–phase characteristics.

For in-plane vibration, the excitation frequency is far below the resonance, so they may be regarded as non-resonant.

While the frame is rotating, in-plane vibration of input tines is governed by the two neighbouring modes 3 and 4. The vibration law of output tines depends upon the mutual position of values of natural frequencies f_3 and f_4 on the frequency axis.

If $f_3 = f_4$, the out-of-plane vibration of output tines will not be excited because the contributions of modes 3 and 4 of eliminate each other. However, the resonant out-of-plane vibration will be excited in the input tines. This mode of operation is based on a very narrow allowable frequency range in order to keep the output vibrations essentially on the peak of AFCH curve. Similar dynamic properties can be obtained in case when the transducer is excited over its entire surface. In a rotating frame, the in-plane vibration would excite only the mode 3 of out-of-plane vibration.

The optimum separation of modal frequencies f_3 and f_4 by selecting proper geometrical parameters allows obtaining the out-of-plane vibration of output tines, the AFCH of which has a plateau or a local minimum on its top. Thus the tolerance of the excitation frequency is allowable in a wider range, Fig. 9a,b, where $\overline{U}_A, \overline{U}_B$ and ϕ_A, ϕ_B denote the amplitudes and phases of input and output tines' vibration.

If f_3 is very close but not equal to f_4, and $f_3 < f_4$, the out-of-plane vibration of output tines will be excited by the rotation of the frame. The phase of vibration of output tines will depend upon the mutual positions of natural frequencies of symmetrical (f_3) and anti-symmetrical (f_4) out-of-plane modes on the frequency axis. If the natural frequency of symmetrical mode f_3 because of some constructional factors becomes greater than the natural frequency f_4 of the anti-symmetrical mode, the phase angle of the vibration of the output tines changes through value π, Fig. 9c,d. This leads to the same effect as the change of the sign of the angular rate of the frame rotation and may cause misinterpretations of the direction of rotation.

By ensuring an appropriate separation between modal frequencies of the out-of-plane vibration of the transducer, the peaks of the AFCH may be made wider and less sharp in order to decrease the possibility of misinterpretation of the measured angular rate direction that is identified on the base of the phase angle of vibration of the output tines.

8. Conclusions

Structural vibration problems present certain design limitations necessary for ensuring a correct interpretation of the properties of the system.

A computation model and software tools have been developed for the analysis of the dynamic behaviour of the balanced H-shape oscillator of the piezoelectric angular rate sensor by using the finite element method and by including the gyroscopic effects caused by the rotation of the reference frame. The model is capable of predicting the system's behaviour and characterizing comprehensively the system by taking into account both static and dynamic disturbances and parameter deviations.

It has been demonstrated that the dynamic analysis of the angular rate sensor by employing the 3D FE model facilitates considerably the understanding the peculiarities of the operation of the sensor and allows the quantitative evaluation of the input–output relationship. The main operational modes of the angular rate sensor have been analyzed and optimum separation of the modal frequency values have been found ensuring a correct interpretation of the direction of the measured angular rate.

The modelling approach presented can be also employed during the education of advanced level specialists in the field of measurement and instrumentation in the design-oriented framework.

References

[1] F. Abdullah, L. Finkelstein, S.H. Khan, W.J. Hill, Modelling in measurement and instrumentation – an overview, Measurement 14 (1994) 41–54.

[2] J. Maryska, J. Novak, P. Ralek, Modelling of piezoelectric resonators, in: Proceedings of the Sixteenth Eurosensors Conference, Prague, Czech Republic, 2002, pp. 144–145.

[3] I. Hopkins, Performance and design of a silicon micromachined gyro. Available from: interrefhttp://www.siliconsensing.comurl<http://www.siliconsensing.com>, pp. 6.

[4] W. Geiger, B. Folkmer, J. Merz, H. Sandmaier, W. Lang, A new silicion rate gyroscope, Sensors and Actuators 73 (1999) 45–51.

[5] Y. Nonomura et al., Quartz rate gyro sensor for automotive control, in: Proceedings of the Sixteenth Eurosensors Conference, Prague, Czech Republic, 2002, pp. 816–817.

[6] A. Madni, R. Geddes, A Micromachined quartz angular rate sensor for automotive and advanced inertial applications. Available from: <http://www.sensorsmag.com/articles/0899>.

[7] J. Webster (Ed.), The Measurement, Instrumentation, and Sensors Handbook, CRC Press LLC, 1999.

[8] S. Kaušinis, R. Barauskas, Simulation of an angular velocity sensor, in: Proceedings of the IMEKO Symposium Virtual and Real Tools for Education in Measurement, University of Twente, Enschede, the Netherlands, 2001, pp. 95–101.
[9] S. Kaušinis, R. Barauskas, Computer modelling of a piezoelectric angular rate sensor, in: Proceedings of the XVII IMEKO World Congress, Dubrovnik, Kroatia, 2003, pp. 1088–1093.
[10] R. Barauskas, Techniques in the dynamic analysis of structures with unilateral constraints, in: Structural Dynamic Systems Computational Techniques and Optimization: Nonlinear Techniques, Gordon and Breach Science Publishers, 1999, pp. 131–194.